Spontaneous Vesicle Formation of Single Chain and Double Chain Cationic Surfactant Mixtures

Makoto Aratono,*,† Nami Onimaru,† Yumi Yoshikai,† Makiko Shigehisa,† Ikuyo Koga,† Kanda Wongwailikhit,‡ Akio Ohta,§ Takanori Takiue,† Belkoura Lhoussaine,|| Reinhard Strey,|| Youich Takata,† Masumi Villeneuve,⊥ and Hiroki Matsubara†

Department of Chemistry, Faculty of Sciences, Kyushu University, Fukuoka 812-8581, Japan, Chemistry Department, Faculty of Science, Rangsit University, Patumtani, 12000, Thailand, Department of Chemistry and Chemical Engineering, Faculty of Engineering, Kanazawa University, Kanazawa 920-1192, Japan, Institute of Physical Chemistry, University of Cologne, Cologne, D-500939 Germany, and Department of Chemistry, Faculty of Science, Saitama University, Saitama 338-8570, Japan

Received: June 15, 2006; In Final Form: October 30, 2006

The concentration vs composition diagram of aggregate formation of the dodecyltrimethylammonium bromide (DTAB) and didodecyldimethylammonium bromide (DDAB) mixture in aqueous solution at rather dilute region was constructed by analyzing the surface tension, turbidity, and electrical conductivity data and inspected by cryo-TEM images and dynamic light scattering data. Although the aqueous solution of DTAB forms only micelles, the transition from monomer to small aggregates and then to vesicle was found at $0.1 < X_2 \leq 1$, where X_2 is the mole fraction of DDAB in the DTAB−DDAB mixture, while vesicle particles were formed directly from monomer solution at $0 < X_2 < 0.1$. Furthermore, the transition from vesicle to micelle was found at $0 < X_2 < 0.4$ at higher concentrations. An addition of DTAB to DDAB solution lowered considerably the DDAB concentration of the vesicle formation, which is attributable to asymmetric distribution of DTAB molecules between inner and outer monolayers of the vesicle bilayer. The shape and size of aggregates were obtained from surface tension, cryo-TEM, and light scattering data.

Introduction

Surfactant molecules gather together to form a variety of aggregates with different geometries and dimensions owing to changes in chemical structure of molecules, concentrations, mixing ratios for multicomponent systems, temperatures, pressures, and so on in aqueous solutions.[1−3] Among them, vesicle is one of the typical types of aggregates. It has been believed that an external perturbation such as sonication or solvent extraction is required to form vesicle particles from open lamella surfactant bilayers because the inner and outer monolayes have to have an opposite sign of curvature. Nevertheless, the spontaneous vesicle formation of dialkyldimethylammonium hydroxide was disclosed at higher pH by using cold-stage electron microscopy by Talmon et al.[4] Since then the spontaneous vesicle formation has been demonstrated for dialkyldimethylammonium bromide,[5−8] and double tailed biological amphiphile with a saccharidic head group ganglioside GM3.[9] Svitova et al. have studied the formation of aggregates of dialkyldimethylammonium bromide in dilute aqueous solutions by surface and interfacial tensions as well as light scattering, densitometry, and freeze-fracture electron microscopy and concluded that there are vesicle and multilamellar aggregates.[8]

The spontaneous vesicle formation of a single surfactant system has been explained as, for an example, that the formation of a closed spherical bilayer becomes more favorable both energetically and entropically than that of infinite planner bilayers; the energetically unfavorable edges are eliminated in a closed bilayer at a finite, rather than infinite, aggregation number.[10] For appropriate mixed surfactant systems, however, the spontaneous vesicle formation probably can take place more easily, because the inner and outer monolayers can have different surfactant compositions and thus different signs of curvature from each other. Bergström has investigated the influence of surfactant mixing on the curvature free energy of a thermodynamically open and reversibly formed vesicle bilayer by deriving expressions for the various contributions to the bilayer bending constant.[11] Thus there are many more reports on vesicle formation of surfactant mixtures compared to that of single surfactant systems. Typical binary surfactant systems spontaneously forming vesicles are ion pair ($R_1^+ R_2^-$),[12] catanionic ($R_1^+ X^- + M^+ R_2^-$),[13−22] and bicationic ($R^+ X^- + (R_1R_2)^+ Y^-$) surfactants.[15,23] Although the first system is not a surfactant mixture, but counterions X^- and M^+ are removed from the catanionic surfactant, the inner and outer monolayers can have different compositions.

In our previous paper on vesicle formation of the $R_1^+ X^- + M^+ R_2^-$ system,[17] the surface tension and densitometry showed thermodynamically that vesicles are formed spontaneously and can coexist with normal micelles within a limited range of the total concentration and mixing ratio of the surfactant mixture. A simple model on the concentration vs composition diagram was proposed and verified to be useful to understand the phase behavior of the mixture. Furthermore, cryo-TEM images clearly demonstrated the existence of vesicle particles. Furthermore, the vesicle formation of the $R_1^+ R_2^-$ system[12] and the effect of

* Address correspondence to this author. E-mail: m.arascc@mbox.nc.kyushu-u.ac.jp.
† Kyushu University.
‡ Rangsit University.
§ Kanazawa University.
|| University of Cologne.
⊥ Saitama University.

10.1021/jp0637328 CCC: $37.00
Published on Web 12/10/2006

equimolar inorganic salt on it[24] were investigated by surface tension, electrical conductivity, and cryo-TEM images. A multilamellar vesicle was formed in these systems and it was found that an addition of the inorganic salts to the $R_1^+R_2^-$ system reduced the electrostatic interaction between cationic and anionic surfactant ions and, therefore, the critical vesicle concentration was increased.

In the present paper, the aggregate formation of the bicationic surfactant system of $R^+X^- + (R_1R_2)^+Y^-$ as a function of the mixing ratio and total concentration of two surfactants is investigated in detail, where R^+X^- and $(R_1R_2)^+Y^-$ are respectively dodecyltrimethylammonium bromide and didodecyldimethylammonium bromide, by measuring surface tension γ, turbidity τ, and electrical conductivity κ and analyzing the data. The main purposes are to construct the concentration vs composition diagram that displays the boundaries between different aggregation states on the basis of the γ, τ, and κ data and to inspect the diagram by examining cryo-TEM images and dynamic light scattering, and then to clarify the geometry and sizes of aggregates.

Experimental Section

Materials. DTAB purchased from Tokyo Kasei Kogyo Co., Ltd. (Japan) was recrystalillized three times from an acetone/ethanol mixture of 5/1 volume ratio and dried in vacuo. DDAB was purchased from ACROS Organics (USA) and recrystallized from ethyl acetate. Their purity was checked by surface tension measurements of their aqueous solutions at 298.15 K and confirmed by observing no minimum on the surface tension vs concentration curves around the critical micelle concentration (cmc). Water used for the surface tension, turbidity, and conductivity measurements was distilled three times from alkaline permanganate solution.

Surface Tension. Surface tension γ was measured by the drop volume[25,26] and pendent drop[27,28] methods at 298.15 K under atmospheric pressure as a function of the total molality of constituent ions, $\hat{m}$, defined by

$$\hat{m} = m_{DDA^+} + m_{DTA^+} + m_{Br^-} = 2m_1 + 2m_2 \qquad (1)$$

and the mole fraction of ions dissociated from DDAB, $\hat{X}_2$, defined by

$$\hat{X}_2 = 2m_{DDA^+}/\hat{m} = 2m_2/\hat{m} \qquad (2)$$

where m_1 and m_2 are the molalities of DTAB and DDAB, respectively. The superiority of $\hat{m}$ and $\hat{X}_2$ over the usual definitions of $m = m_1 + m_2$ and $X_2 = m_2/m$ is explained in previous papers.[29,30] In the following, however, we use symbols m and X_2 instead of $\hat{m}$ and $\hat{X}_2$ for simplicity. The error of surface tension measurement was within 0.05 mN m^{-1}.

Turbidity. Turbidity τ was measured by the turbidimeter (HACH 200P) base on the ratio nephelometric method and defined by

$$\tau = I_{90}/(d_1 I_t + d_2 I_{90}) \qquad (3)$$

where I_{90} and I_t are the detector currents of the scattered light at 90° and the transmitted one, and d_1 and d_2 are calibration constants. The experimental error was within 1% of τ values or 0.01 nephelometric turbidity unit (NTU). Solutions to be measured were left standing in an air-conditioned room at least 2 days before the measurements to yield a constant value of τ. For isotropic and dilute solutions, τ is written in terms of particle radius a, number of particles per unit volume N_V, wave length of unpolarized incident light λ, and refractive index of particles relative to the surrounding medium n by[31,32]

$$\tau = (128\pi^5 a^6 N_V/3\lambda^4)(n^2 - 1)/(n^2 + 1) \qquad (4)$$

Thus τ is more sensitive to the change of radius than the number of particles in the solution.

Conductivity. Conductivity κ was measured by the conductometer (CM-60G. TOA-DKK Ltd.) every 10 min for 30 min for a given solution and its experimental error was within 0.5% of the full scale. The measurement was done successively from a concentrated solution to the diluted one by adding pure water or from a lower one to the higher one by adding a concentrated solution at a given X_2. To determine transition points from one solution state to another, the differential conductivity κ_m defined by

$$\kappa_m = (\partial\kappa/\partial m)_{T,p,X_2} \approx (\Delta\kappa/\Delta m)_{T,p,X_2} \qquad (5)$$

was preferably employed, instead of κ itself.[7]

Cryogenic Transmission Electron Microscopy (Cryo-TEM). High-resolution direct cryo-TEM images of molecular aggregates were taken by the transmission electron microscope (LEO EM 912 Omega, Germany) with a stage cooled by liquid nitrogen to −175 ° C. A thin layer of liquid sample suspended on a holey carbon grid was plunged into liquid ethane after the excess liquid was removed by a filter paper.[33,34]

Dynamic Light Scattering (DLS). Dynamic light scattering measurement was carried out in homodyne mode by an ALV-5000 spectrometer (ALV-GmbH, Germany) on the same solutions as the cryo-TEM experiments were performed on. The light source was an argon-ion laser operating at the wave length of 488 nm with vertical polarized light. The decay of correlation function for polydisperse solution is usually described by

$$g(\tau) = \int_0^\infty G(\Gamma)\exp(-\Gamma\tau)\,d\Gamma \qquad (6)$$

where Γand $G(\Gamma)$ are the relaxation rate and its distribution. With use of the mean values of Γ, the translational diffusion coefficient D_0 is evaluated and then the particle hydration radius R_h is calculated through the Stokes−Einstein equation

$$R_h = kT/6\pi\eta D_0 \qquad (7)$$

where η is the viscosity of the solvent. The decay of the correlation function was described in almost all cases by using two components of fast and slow modes in the present study.

Results and Discussion

Surface Tension. The surface tension γ was measured as a function of total molality m at fourteen X_2 values. The γ versus m plots obtained were shown in Figure 1 and classified into four groups according to their common feature: Group A ($X_2 = 0$), Group B ($X_2 = 0.00025, 0.0005, 0.001, 0.002, 0.004, 0.05, 0.1$), Group C ($X_2 = 0.2, 0.3$), Group D ($X_2 = 0.4, 0.6, 0.8, 1$). The representatives for each group are demonstrated in Figure 2.

The curve at $X_2 = 0$ (pure DTAB) belongs to Group A. The surface tension decreases rapidly with increasing m and is almost constant above the break point (a) around 30 mmol kg^{-1} corresponding to a usual cmc. This is a typical surface tension behavior of normal micelle forming systems. Group D has four curves including that of the pure DDAB system. The surface tension decreases rapidly at lower concentration up to the first break point (c), then gradually goes down above it, and becomes

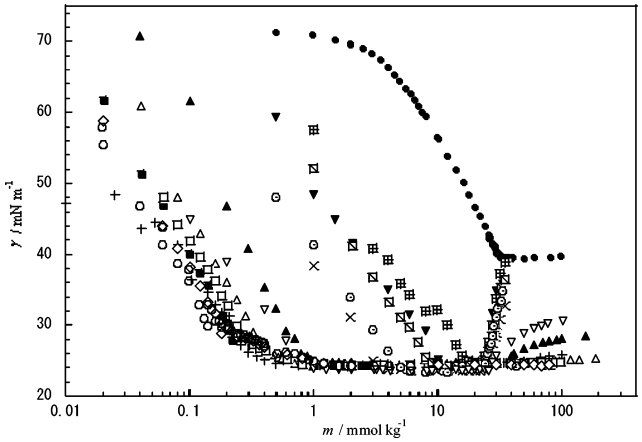

Figure 1. Surface tension vs molality curves at constant compositions. Group A: (●) $X_2 = 0$ (DTAB); Group B: (⊞) 0.00025, (▼) 0.0005, (⊠) 0.001, (⊙) 0.002, (×) 0.004, (▽) 0.05, (▲) 0. 1; Group C: (+) 0.2, (△) 0.3; Group D: (□) 0.4, (■) 0.6, (◇) 0.8, (○) 1 (DDAB). It should be noted that m and X_2 are defined by eqs 1and 2, respectively.

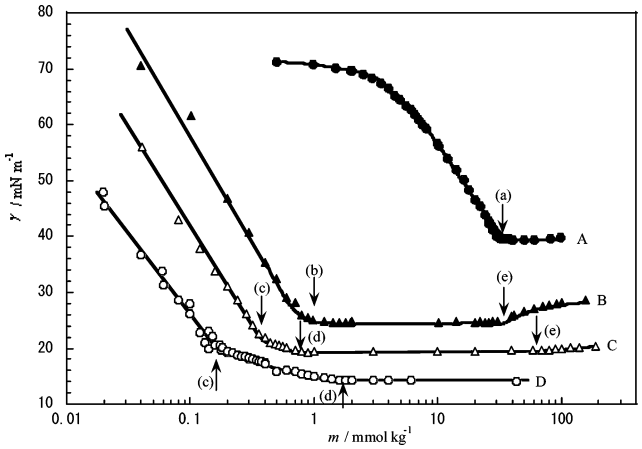

Figure 2. Surface tension vs molality curves of the representatives of each group. The symbols are the same as in Figure 1. The curves of C and D are shifted downward by 5 and 10 mN m^{-1}, respectively.

constant above another break point (d). The solution was transparent up to a little below (d) and then became turbid. Thus it was suggested that vesicle particles are formed at the higher concentration above (d), which was later confirmed by the cryo-TEM image. The slow decrease of γ in the region between (c) and (d) hints a formation of aggregates that are composed of a small number of molecules. According to the thermodynamic consideration on adsorption from small aggregate solutions,[35] the ratio $\partial\gamma/\partial \log m$ just below and above the break point approximately gives an average aggregation number by

$$\bar{N} = (\partial\gamma/\partial \log m)_{m<\mathrm{cmc}}/(\partial\gamma/\partial \log m)_{m>\mathrm{cmc}} \qquad (8)$$

under the assumptions that distribution of aggregation number is very small and the adsorption does not change after the cmc. $\bar{N}$ was found to be around 4−10 for curve D. Referring to that vesicle particles are formed at higher concentrations, small aggregates may be a kind of embryo of a vesicle, like an interdigitated bilayer fragment.

The curves of Group B showed two distinct break points. The surface tension decreases rapidly below the first break point (b). It was almost constant and the solution was turbid between (b) and (e), which suggests vesicle formation. Above (e) it increased with m and the solution was completely transparent, which suggests that vesicle particles have disappeared and

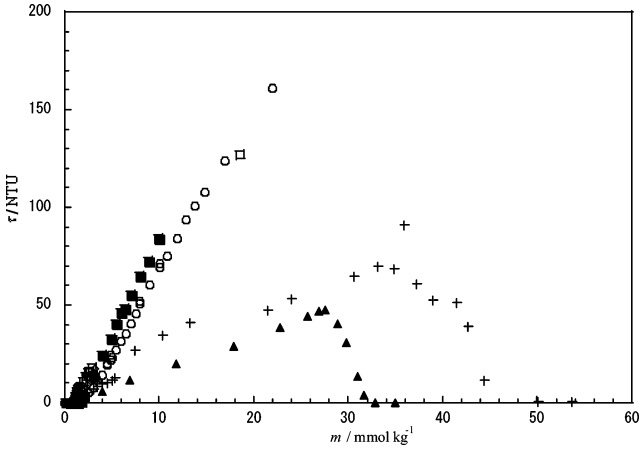

Figure 3. Turbidity vs molality curves at constant compositions. Group A: not shown here because τ is less than 0.1 at all concentrations; Group B: (▽) 0.005, (▲) 0. 1; Group C: (+) 0.2; Group D: (▼) 0.5, (□) 0.7, (◇) 0.8, (■) 0.9, (○) 1 (DDAB).

dissociated into monomers, small aggregates, or micelles. From the views that γ does not decrease, but increases with concentration and that the concentration at (e) is close to that at the cmc of pure DTAB and X_2 values of this group are all small, the conversion into micelles is probable. Furthermore, from the thermodynamic consideration on micelle and vesicle formation from surfactant mixtures,[17,36] the constant surface tension between (b) and (e) indicates that either composition of vesicles does not change with m or two kinds of large size aggregates, that is, vesicle and micelle in the present case, coexist in the solution, while the increase above (e) shows that the composition of micelle changes appreciably in this concentration region. The curves in Group C have the characteristics of both Groups B and D.

In this way, we have assigned the solution states from the characteristics of surface tension behavior and the thermodynamic consideration on them. Let us put our thoughts together as (a) monomer to micelle, (b) monomer to vesicle, (c) monomer to small aggregate, (d) small aggregate to vesicle, and (e) vesicle or vesicle + micelle coexistence to micelle.

Turbidity. The turbidity τ was measured as a function of m at nine X_2. The plots are given in Figure 3 and classified into four groups according to their common feature: Group A ($X_2 = 0$), Group B ($X_2 = 0.05$, 0.1), Group C ($X_2 = 0.2$), and Group D ($X_2 = 0.5$, 0.7, 0.8, 0.9, 1). Turbidity at $X_2 = 0$ (pure DTAB) was less than about 0.1 at all concentrations and not shown in Figure 3.

The representatives for three groups are demonstrated in Figure 4. At $X_2 = 0.1$ of Group B, τ started to increase at (b) and then decrease at (g), and became almost zero at (e). The concentrations at (b) and (e) almost coincide with those determined in the surface tension curves and thus it is said that vesicle particles start to appear at (b) and disappear at (e). The decrease in τ from (g) implies that the number and/or size of vesicle particles is decreasing, while the number of micelle particles is increasing from (g) to (e). Therefore the constant surface tension between (b) and (e) at $X_2 = 0.1$ is due to the size of vesicles being large enough for γ to be constant between (b) and the concentration corresponding to (g) and that, on the other hand, vesicle coexists with micelle between (g) and (e), respectively.

At $X_2 = 1$ of Group D, τ started to increase at (d) and the τ versus m curve has a break point at (f). Judging from the fact that the concentrations at (d) on the surface tension and turbidity curves coincide with each other, it is said that vesicle formation

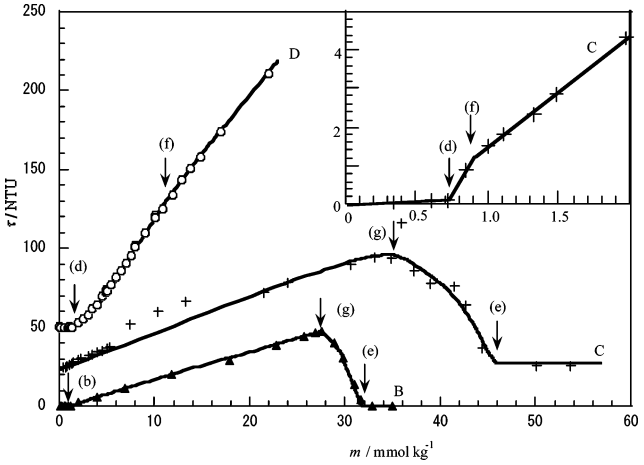

Figure 4. Turbidity vs molality curves of the representatives of each group. The symbols are the same as in Figure 3. The curves C and D are shifted upward by 25 and 50 NTU, respectively.

begins at (d). Since the surface tension curve suggested small aggregate formation at concentrations above (c) of which concentration is smaller than that of (d), it is said that vesicle particles coexist with small aggregate between (d) and (f) and then small aggregates disappears around (f) and the solution contains only vesicles and monomer. The curve at $X_2 = 0.2$ of Group C has four break points. It demonstrates a similarity to the curve of $X_2 = 1$ at a lower m with respect to (d) and (f) as shown by the inserted figure and also to the curve at $X_2 = 0.1$ at a higher m with respect to (g) and (e), respectively. Here it should be noted that τ values themselves and its dependence on m in the vesicle existence region at $X_2 = 1$ is fairly large compared to those at $X_2 = 0.1$ and 0.2. Considering that τ is more sensitive to the change of radius than to the number of particles in the solution, the finding suggests a large size of pure DDAB vesicles compared to those of the mixture.

Summarizing the results of the turbidity experiments, the coexistence region of small aggregate and vesicle and that of vesicle and micelle were furthermore identified between (d) and (f) and between (g) and (e), respectively. Furthermore, the vesicle size is suggested to be dependent on X_2.

Conductivity. The specific conductivity κ was measured as a function of m at twelve X_2 values and the κ vs m plots are shown in Figure 5. We notice at first glance that the plots in Figure 5a seem to have characteristic features for micelle forming ionic surfactants and, however, the plots except at $X_2 = 1$ in Figure 5b exhibit a decrease of κ with increasing ionic surfactant concentration. To specify transition concentrations and understand solution states from the conductivity data, however, the differential conductivity defined by eq 5 is more useful than $\kappa = \sum_i c_i\lambda_i$ itself because[7,37]

$$\kappa_m = \sum_i c_i(\partial\lambda_i/\partial m) + \sum_i (\partial c_i/\partial m)\lambda_i \qquad (i = \text{all chemical species}) \quad (9)$$

Thus κ_m is influenced not only by the magnitude of c_i and λ_i but also by their changes with m. Examining closely the κ_m vs m curves, it was found that the conductivity behavior was classified into four groups: Group A ($X_2 = 0$), Group B ($X_2 = 0.001$, 0.1), Group C ($X_2 = 0.2$, 0.3), and Group D ($X_2 = 0.4$, 0.5, 0.6, 0.7, 0.8, 0.9, 1). The representatives of the differential conductivity curve for each group are shown in Figure 6.

At $X_2 = 0$ (pure DTAB), κ_m shows a sigmoidal decrease with an inflection point (a) corresponding to the cmc. The curve at

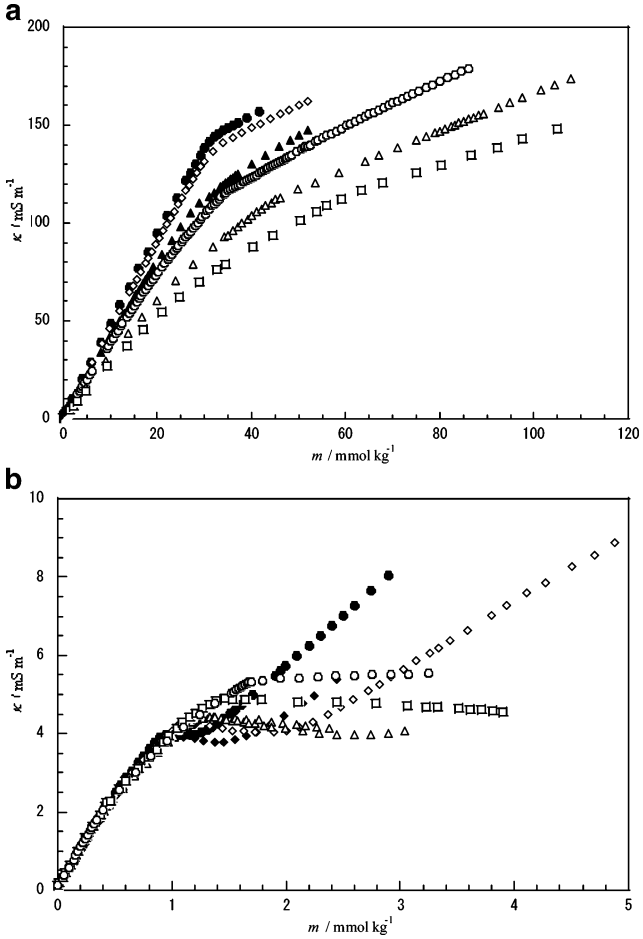

Figure 5. Specific conductivity vs molality curves at constant compositions: (a) (●) $X_2 = 0$ (DTAB), (◇) 0.001, (▲) 0. 1, (○) 0.2, (△) 0.3, (□) 0.4; (b) (●) 0.5, (▲) 0.6, (◇) 0.7, (△) 0.8, (□) 0.9, (○) 1 (DDAB). The curves at $X_2 = 0.5$ to 0.8 have a clear minimum.

$X_2 = 1$ (pure DDAB) has two characteristic points of a very sharp maximum (c) around 0.17 mmol kg^{-1} and an inflection point (d) around 1.6 mmol kg^{-1}. The appearance of the maximum was reported and attributed to formation of small size aggregates.[7,37] The gradual decrease of surface tension in this concentration range and small aggregation number estimated from the surface tension curve support this view as mentioned above. Considering that the solution became bluish and the turbidity started to increase around (d), vesicle formation probably started in the small aggregate solution. The concentration (f) around which small aggregates disappear becomes less prominent with increasing X_2 and was not indistinct, although 11.5 mmol kg^{-1} was determined from the turbidity data, at $X_2 = 1$.

The curve at $X_2 = 0.3$ has three inflection points at (d) 0.8, (f) 0.97, and (g) 43.55 mmol kg^{-1}, respectively. Judging from that the analysis of surface tension curves suggested the formation of a small aggregate at concentrations above 0.38 mmol kg^{-1} and the small aggregate−vesicle coexistence above 0.76 mmol kg^{-1}, it is said that the small aggregate−vesicle coexistence region is ended around (f) and the vesicle−micelle coexistence starts around (g). Although the concentrations of aggregate formation (c) and the end point of the vesicle−micelle coexistence (e) were clearly determined respectively at 0.38 and 80 mmol kg^{-1} from the surface tension curve, they were not evident on the κ_m curve but the curve just showed symptoms as a tiny maximum around 0.33 and a vague inflection point around 80 mmol kg^{-1}(outside the figure), respectively. The

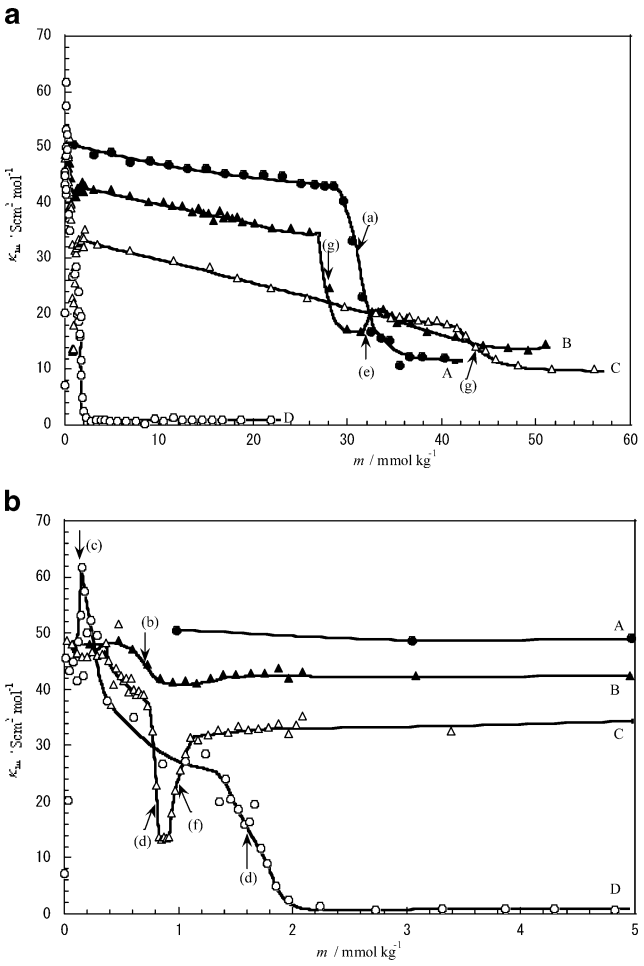

Figure 6. Differential conductivity vs molality curves of the representatives of each group. Group A: (●) $X_2 = 0$ (DTAB); Group B: (▲) 0. 1; Group C: (△) 0.3; Group D: (○) 1 (DDAB).

inflection points (b), (g), and (e) at $X_2 = 0.1$ were respectively assigned as the concentrations of vesicle formation and starting and end points of the vesicle−micelle coexistence, which is consistent with the assignments based on the surface tension and turbidity measurements.

It is seen that κ_m values of vesicle regions change strongly with X_2 from around 40 to almost 0, while those of micelle regions are almost constant. This suggests that the properties of vesicle particles such as size, degree of counterion binding, structures, and so on are dependent strongly on X_2, while those of micelles are not. The former coincides with the indication from the turbidity. Furthermore, it should be noted that κ_m values in the coexistence regions of small aggregate + vesicle between (d) and (f) and vesicle + micelle between (g) and (e) generally become smaller compared to those when solutions contain only a single kind of aggregate. Thus this behavior is a specific one for the coexistence of two kinds of aggregates. Taking note of that κ_m takes even a negative value at $X_2 = 0.5-0.9$, where small aggregates are coexisting with large vesicles, as expected from the κ curves in Figure 5, it is said that ions of monomer, counter bromide, and small aggregate in the inner aqueous solution pool of vesicle particles may not contribute to the electric conductivity of the solution compared to those in the outer aqueous solution.

Thus several kinds of transition points were determined from the conductivity measurements and have good correspondence to the results from the surface tension and turbidity measurements. The changes of γ, τ, and κ_m with the transition of solution

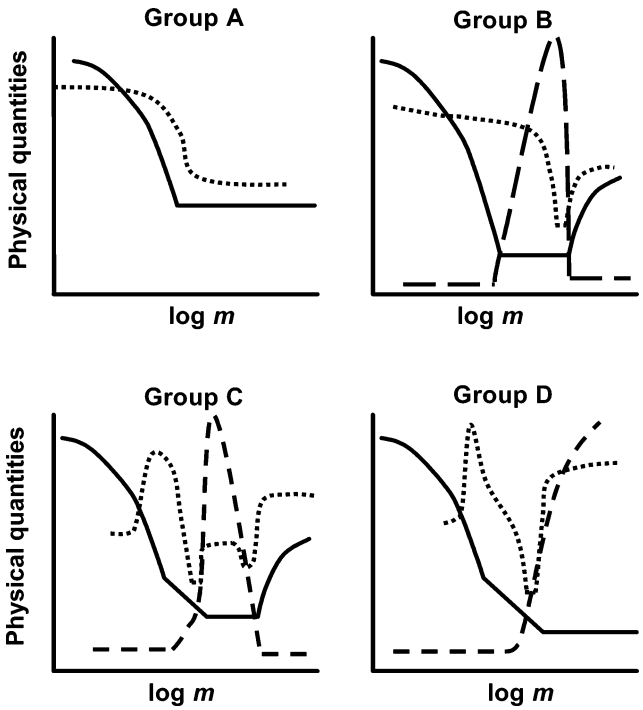

Figure 7. Schematics of the change of physical quantities accompanied by transitions of the solution state of the respective groups: (−) surface tension, (---) turbidity, and (···) differential conductivity.

states are schematically displayed in Figure 7. Although the differential conductivity is most influenced by the transition, it is evident that the others complement each other and, furthermore, the respective methods afford valuable information on the solution state as desribed above.

Concentration Versus Composition Diagram at the Transition Points. The transition concentrations determined are summarized in Table 1. Here m_α^β refers to the molality at the transition point from α to β, and the sub- and superscripts m, A, A+V, V, V+M, and M symbolize monomer, small aggregate, coexistence of small aggregate and vesicle, vesicle, coexistence of vesicle and micelle, and micelle, respectively. The average values of m_α^β yielded from different methods, $\bar{m}_\alpha^\beta$, were employed to construct the concentration versus composition diagram. The $\bar{m}_\alpha^\beta$ values are also summarized in Table 1 and the diagram is demonstrated in Figure 8.

Now let us examine the diagram. In the single component solution of DDAB, the γ, τ, and κ experiments suggest that at first small aggregates and then vesicles are formed. The cryo-TEM image at 6.5 mmol kg^{-1} in the A+V region given in Figure 9(a) demonstrates clearly the existence of large vesicles. Although an existence of small aggregates is still controversial in the literature,[7,8,13−15,38,39] it is obvious from the diagram that the coexistence region extends into the wide range of the DDAB−DTAB mixture, but shrinks gradually with increasing the proportion of DTAB and eventually disappears around $X_2 = 0.1$. It is important to note that the vesicle region reaches to a composition very close to single DTAB solution and furthermore vesicles are formed directly from monomeric solutions of DTAB and DDAB mixtures at $X_2 < 0.1$. The decrease in $\bar{m}_{A+V}^{V}$ with the addition of DTAB molecules demonstrates that vesicle particles are more easily formed in the presence of single chain surfactant.

At the higher m and lower X_2 region, the experiments showed that micelle particles start to form in the vesicle solution at around $\bar{m}_V^{V+M}$ and vesicle particles ultimately disappear at

around $\bar{m}^{M}_{V+M}$ after passing through the vesicle+micelle coexistence region with increasing the total surfactant concentration m. This behavior seems to be unusual for single surfactant systems that exhibit vesicle formation, such as DDAB, but unique for binary surfactant mixtures such as catanionic ($R_1^+ X^- + M^+ R_2^-$)[17] and bicationic ($R^+ X^- + (R_1R_2)^+ Y^-$) ones. In the bicationic mixtures, the geometry of the $(R_1R_2)^+$ ion is favorable for vesicle formation at relatively lower concentrations and R^+ ions form micelle at relatively higher concentrations: since vesicle particles abound more in $(R_1R_2)^+$ ions, as expected from their geometry and proved later, compared to R^+ ions, R^+ ions left over in the solution start to form micelles when the concentration of the monomeric form of the R^+ ion reaches that sufficient for micelle formation. The concentration vs composition diagram clearly demonstrates that both $\bar{m}^{V+M}_{V}$ and $\bar{m}^{M}_{V+M}$ go up with adding DDAB molecules. This strongly suggests that DDAB molecules are incorporated into micelle particles to some extent and, furthermore, the increase in γ above (e) of Group B in Figures 1 and 2 confirms that the composition of micelle changes gradually with m at a given X_2. For the catanionic system, the ion pair $R_1^+ R_2^-$ is favorable for vesicle formation, like $(R_1R_2)^+$, and R_1^+ or R_2^- become excess over $(R_1R_2)^+$, like R^+ in the bicationic system, at compositions except 0.5. Thus the situation of the catanionic system except for its equimolar mixture is similar to that of a bicationic system. This was demonstrated in our previous paper.[17]

Since the single component solution of DTAB forms only spherical micelle, it is important to examine in what way the micelle and vesicle regions are connected with each other. The transition concentrations $\bar{m}^{V}_{m}$ and $\bar{m}^{M}_{V+M}$ are plotted at low X_2 region in Figure 8b, where $\bar{m}^{V+M}_{V}$ was not measured in the composition region given here. The extrapolation of the $\bar{m}^{V}_{m}$ and $\bar{m}^{M}_{V+M}$ curves hit at point (t); the composition X_2 and total molality m of (t) are about 0.00015 and 20 mmol kg^{-1} and are denoted in the following by $X_2^{m,t}$ and $m^{m,t}$, respectively. This

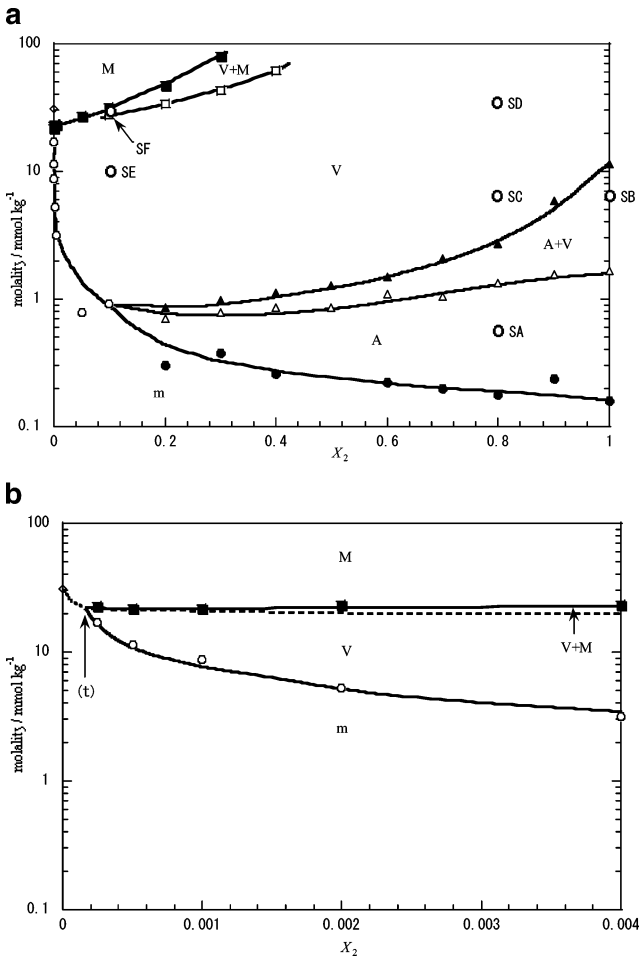

Figure 8. Concentration vs composition diagrams of aggregate formation. (●) $\bar{m}^{A}_{m}$, (○) $\bar{m}^{V}_{m}$, (◇) $\bar{m}^{M}_{m}$, (△) $\bar{m}^{A+V}_{A}$, (▲) $\bar{m}^{V}_{A+V}$, (□) $\bar{m}^{V+M}_{V}$, and (■) $\bar{m}^{M}_{V+M}$.

TABLE 1: The Concentration Values at the Phase Boundaries Determined by Three Methods and Their Average Values.

		$X_2 =$																
		0	0.0003	0.0005	0.001	0.002	0.004	0.05	0.1	0.2	0.3	0.4	0.5	0.6	0.7	0.8	0.9	1
m^{M}_{m}	γ	30.80																
	κ	30.80																
	τ																	
	av	30.80																
m^{V}_{m}	γ		17.10	11.45	8.80	5.25	3.20	0.85	1.00									
	κ								0.72									
	τ							0.70	1.00									
	av		17.10	11.45	8.80	5.25	3.20	0.78	0.91									
m^{M}_{V+M}	γ		22.50	21.80	21.90	23.00	23.40	27.10	32.00	48.80	80.00							
	κ				(30.92)				32.00	(47.00)	80.00							
	τ									46.00								
	av		22.50	21.80	21.90	23.00	23.40	27.10	32.00	47.40	80.00							
m^{V+M}_{V}	γ										(40.00)							
	κ								28.00	33.00	43.55	61.21						
	τ								27.60	35.00								
	av								27.80	34.00	43.55	61.21						
m^{V}_{A+V}	γ													(1.41)				
	κ									0.85	0.97	1.11	1.28	1.50	2.00	3.20	5.90	11.54
	τ									0.87			1.30		2.20	2.27	5.80	
	av										0.97	1.11	1.29	1.50	2.10	2.74	5.85	
m^{A+V}_{A}	γ									0.43	0.76	0.80		1.20		1.59		1.68
	κ									0.70	0.80	0.89	0.92	1.00	1.10	1.20	1.45	1.63
	τ									0.72			0.80		1.00	1.27	1.68	1.62
	av									0.71	0.78	0.85	0.86	1.10	1.05	1.35	1.57	1.65
m^{A}_{m}	γ									0.30	0.38	0.27		0.22		0.18		0.16
	κ										(0.33)	0.25	(0.28)	(0.22)	0.20	0.18	0.24	0.17
	τ																	
	av									0.30	0.38	0.26		0.22	0.20	0.18	0.24	0.17

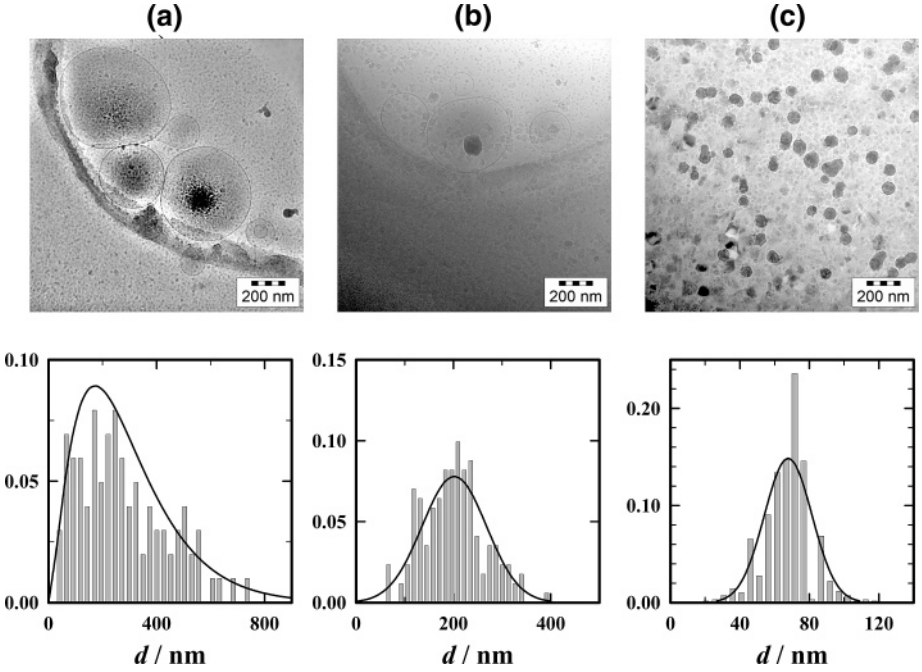

Figure 9. Cryo-TEM images and size distribution of vesicles: (a) $X_2 = 1$, $m = 6.5$ mmol kg^{-1}; (b) $X_2 = 0.8$, $m = 6.0$ mmol kg^{-1}; and (c) $X_2 = 0.1$, $m = 9.9$ mmol kg^{-1}.

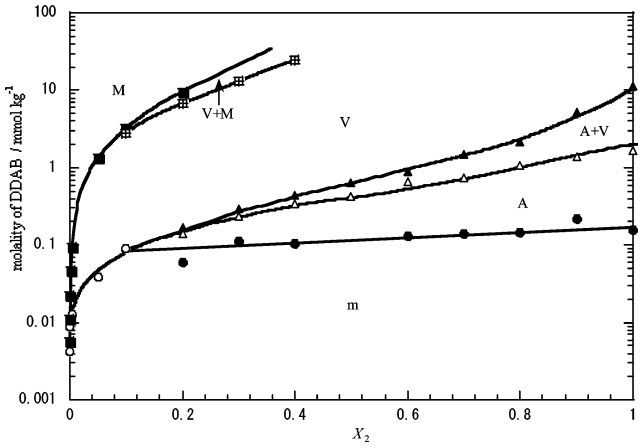

Figure 10. Concentration of DDAB vs composition diagrams of aggregate formation: (●) $\bar{m}^{A}_{m,2}$, (○) $\bar{m}^{V}_{m,2}$, (△) $\bar{m}^{A+V}_{A,2}$, (▲) $\bar{m}^{V}_{A+V,2}$, (□) $\bar{m}^{V+M}_{V,2}$, and (■) $\bar{m}^{M}_{V+M,2}$.

result is particularly surprising in view that the monomer concentration of DDAB at (t) is about $20 \times 0.00015 = 3 \times 10^{-3}$ mmol kg^{-1} and vesicles are formed even up to this extremely low DDAB concentration compared to the critical vesicle concentration of the single DDAB solution (1.65 mmol kg^{-1}). These findings indicate that addition of single chain DTAB makes it easy for DDAB molecules to form vesicles and vesicle particles are mainly composed of DDAB molecules.

The former point is clearly demonstrated in the DDAB concentration at the transition point $\bar{m}^{\beta}_{\alpha,2}$ ($=\bar{m}^{\beta}_{\alpha}X_2$) versus X_2 curves shown in Figure 10. The concentration $\bar{m}^{A}_{m,2}$ is almost constant and thus small aggregate formation takes place at a constant chemical potential of DDAB irrespective of the presence of DTAB molecules in the solution. This may suggest that small aggregates are composed of only DDAB molecules. On the other hand, all the values of the DDAB concentration related to vesicle formation, that is, $\bar{m}^{A+V}_{A,2}$, $\bar{m}^{V}_{A+V,2}$, and $\bar{m}^{V}_{m,2}$, are clearly diminished with adding DTAB molecules. Thus vesicles are formed more easily in the presence of single chain DTAB molecules in spite of DTAB not forming vesicles solely, which ensures that DTAB molecules take part in vesicle formation. From this point of view, knowledge on the compositions in the small aggregates and vesicles helps us to understand why the behavior given in Figure 10 is observed. However, it may be almost impossible to directly estimate them from experiments, but only a rough estimation of the composition of aggregates in terms of the excess aggregation number is utilized[29] as follows.

Let us define the composition of DDAB in aggregated state X_2^{α} by

$$X_2^{\alpha} = N_2^{\alpha}/(N_1^{\alpha} + N_2^{\alpha}) \tag{10}$$

where N_i^{α} is the excess number of surfactant ions i defined with respect to appropriate dividing surfaces.[17,29,36] X_2^{α} is estimated from the dependence of the $\bar{m}^{V}_{\mathbf{m}}$ and $\bar{m}^{A}_{m}$ values on m by using the equation

$$X_2^{\alpha} = X_2 - 2X_1(\partial \ln \bar{m}^{\alpha}_{m}/\partial \ln X_2)_{T,p} \tag{11}$$

for the present mixture. The best fitted linear plots for the ln $\bar{m}^{V}_{m}$ versus ln X_2 and ln $\bar{m}^{A}_{m}$ versus ln X_2 gave the slope $\partial \ln \bar{m}^{V}_{m}/\partial \ln X_2 = -0.528$ with the residual of 0.99 and $\partial \ln \bar{m}^{A}_{m}/\partial \ln X_2$ with that of 0.98, respectively. Thus we have $X_2^{A} = 1 + 0.346X_1$ at $X_2 > 0.1$ for small aggregates and $X_2^{V} = 1 + 0.056X_1$ at $X_2 < 0.1$ for vesicles, respectively. Taking account of eq 10, the larger values of X_2^{A} and X_2^{V} than unity imply that the excess quantity N_1^{α} is negative and thus the concentration of DTAB in and around aggregates α is strongly reduced from that in the bulk monomer solution. Therefore the almost constant value of $\bar{m}^{A}_{m,2}$ indicates that small aggregates are actually composed of DDAB molecules and thus, furthermore, $X_2^{V} < X_2^{A}$ suggests that vesicle particles actually contain DTAB molecules to some extent. The fact that $\bar{m}^{V}_{m,2}$ changes with X_2 supports this view.

Although $\bar{m}^{V+M}_{V}$ was not measured at very low X_2 in the present experiments as mentioned above, it is roughly calculated as a function of X_2 by using the mass balance equation (see the

Appendix) as

$$m_V^{V+M} = [X_2^{m,t}/X_2 + (X_2 - X_2^{m,t})X_2^{V,t}/(X_2^{V,t} - X_2)X_2]m^{m,t} \quad (12)$$

where $X_2^{m,t} = 0.00015$, $m^{m,t} = 20$ mmol kg^{-1}, and $X_2^{V,t}$ is the composition of the vesicle at transition point (t) that is almost unity from the equation $X_2^{V,t} = 1 + 0.056X_2^{m,t}$ given above. The results are plotted in Figure 8b by the dotted line; the m_V^{V+M} value is a little smaller than $\bar{m}_{V+M}^{M}$ at a given X_2 and $m_V^{V+M} = 22$ is close to the experimentally obtained value of 27.8 at $X_2 = 0.1$. Similarly we have the relation about m_{V+M}^{M} as

$$m_{V+M}^{M} = [X_2^{m,t}/X_2 + (X_2 - X_2^{m,t})X_2^{M,t}/(X_2^{M,t} - X_2)X_2]m^{m,t} \quad (13)$$

This equation shows that the m_{V+M}^{M} value diverges to infinity as X_2 approaches the micelle composition at transition point (t) $X_2^{M,t}$. Since the experiments demonstrated that $\bar{m}_{V+M}^{M}$ is finite at least up to about $X_2 = 0.3$, it is concluded that $X_2^{M,t}$ is larger than 0.3. This confirms that micelle particles contain a considerable number of DDAB molecules.

Size and Morphology of Aggregates. Aggregates in the A region are expected to be small with $\bar{N} = 4-10$ from the surface tension measurements and actually the solution at point SA ($X_2 = 0.8$, $m = 0.59$ mmol kg^{-1}) in this region showed no detectable intensity in the DLS measurement. Although there is no direct information on their morphology, we suspect that they are a kind of embryo of a vesicle like an interdigitated bilayer fragment, because they are almost completely composed of DDAB molecules, and invariably grow up to bilayer vesicles at higher concentrations, and furthermore interdigitation makes the water/hydrocarbon contact area diminish.

In the A+V region at point SB ($X_2 = 1$, $m = 6.51$ mmol kg^{-1}), although the decay of the correlation function of the DLS measurement was well fitted by using two radii of 14 ± 7 and 281 ± 54 nm, the histogram from cryo-TEM images in Figure 9 exhibits a wide size distribution and gives the mean radius of 287 ± 182 nm. Figure 9a displays a clear image of large vesicles, and other pictures at point SB indicated the existence of smaller vesicles inside larger ones. Viseu et al. observed quite large vesicles and open membranes in the cryo-TEM images of sonicated DDAB solution at $m = 5$ mmol kg^{-1}, which is in the A+V region in our study.[14] It should be noted that, although Viseu et al. described the necessity of sonication for the pure DDAB system to form vesicles, our experiments showed that vesicle particles were observed in the A+V region without sonication, that is, spherical vesicle formation takes place spontaneously even for a one-component DDAB system.

At $X_2 = 0.8$, vesicle size increased with increasing concentration: 264 ± 32 and 355 ± 77 from DLS, 202 ± 66 and 291 ± 213 from cryo-TEM, at 5.97 (point SC) and 32.1 (point SD) mmol kg^{-1}, respectively. At $X_2 = 0.1$, on the other hand, it was almost constant or rather decreased with increasing concentration: 44 ± 5 at 9.9 mmol kg^{-1} (point SE) and 50 ± 5 at 30.09 mmol kg^{-1} (point SF) from DLS, 68 ± 14 at the former, and aggregates were not observed at the latter from cryo-TEM, respectively. The difference between these two X_2 is understandable from the concentration vs composition diagram in Figure 8a that vesicle particles further grow into larger or lamellar ones at $X_2 = 0.8$ and, on the other hand, they change to ordinary micelles with increasing concentration at $X_2 = 0.1$. Furthermore, the sizes at about $m = 6-10$ mmol kg^{-1} are decreased with increasing DTAB composition as 287, 201, and 68 at $X_2 = 1$, 0.8, and 0.1, respectively, from cryo-TEM. This implies that the proportion of DTAB in vesicle particles is increased gradually, which makes the vesicle formation more favorable than does the smaller sizes.

Finally, let us consider the distribution of DTAB and DDAB molecules in outer and inner monolayers in vesicle bilayers. The most prominent feature of the binary surfactant mixture in bilayer formation, being different from a single surfactant system, is that compositions in the outer and inner monolayers could be different from each other. It makes it easier for the outer and inner monolayers to have an opposite sign of curvature and to change their sizes according to physical conditions surrounding them such as temperature, pressure, concentration, and so on. Judging from the molecular geometry of DTAB and DDAB molecules, the mole fraction of DTAB molecules is expected to be larger in outer than in inner monolayers. As mentioned above with respect to Figure 10, the DDAB concentrations, $\bar{m}_{A,2}^{A+V}$ and $\bar{m}_{m,2}^{V}$, and thus the chemical potentials at which vesicle formation starts are diminished with adding DTAB molecules in spite of DTAB molecules not forming vesicles solely. Thus it is sure that DTAB molecules strongly participate in vesicle formation. Considering these things, it may be said that DTAB molecules are incorporated into outer monolayers to some extent (the excess number in outer layers $N_1^{V,O}$ is positive) but excluded from inner monolayers and their vicinities in the inner water pools (the excess number in inner layers $N_1^{V,I}$ is negative). Therefore the estimation given above that X_2^{V} is nearly equal to unity does not mean that DTAB molecules are not contained in vesicle particles, but they actually are contained in outer layers and satisfy the condition $N_1^{V} = N_1^{V,I} + N_1^{V,O} \approx 0$. The magnitude of $N_1^{V,O}$ is increased and thus the size of the vesicle is decreased with increasing the composition of DTAB in the solution, because DTAB molecules are in favor of aggregates having larger curvature like micelles.

In a binary mixture of $R^+ X^- + (R_1R_2)^+ Y^-$ with different counterions, e.g., DTAB + didodecyldimethylammonium chloride (DDAC) and dodecyltrimethylammonium chloride (DTAC) + DDAB, the composition of counterions as well as that of surfactant ions could be different between inner and outer monolayers and thus may give different concentration versus composition diagrams and size and morphology of aggregates from those of the DTAB−DDAB system. Studies on aggregate formation of these systems are important to understand the role of counterions in aggregate formation and are now being performed.

Acknowledgment. This work was supported in part by the Grant-in-Aid for Scientific Research (B) (no. 1635005) and also by the Grant-in Aid for Exploratory Research (no. 17655062). Y.T. acknowledges support from the Grant-in-Aid for JSPS fellows (no. 16·6576).

Appendix

In our previous paper,[17] a simple model of the concentration−composition diagram of aggregate formation was proposed for a binary surfactant mixture of $R_1^+ X^- + M^+ R_2^-$ under the assumption that the monomer concentration did not change appreciably as the total concentration of surfactants was increased. The model was compared with the experimental results. The coincidence between the model and experiments was not so bad. However, the monomer concentration is actually changed with the total concentration and thus it should be taken into account. Here the revised version of the model is proposed.

When vesicle and micelle are coexisting in the solution, the mass conservation is written as

$$mX_2 = m^{\mathrm{m}}X_2^{\mathrm{m}} + m^{\mathrm{V}}X_2^{\mathrm{V}} + m^{\mathrm{M}}X_2^{\mathrm{M}} \tag{A1}$$

and

$$m = m^{\mathrm{m}} + m^{\mathrm{V}} + m^{\mathrm{M}} \tag{A2}$$

Since sizes of micelle and vesicle particles are usually large enough for m^{m}, X_2^{m}, X_2^{V}, and X_2^{M} to be constant when they are defined in terms of excess numbers of constituent species as eq 10 in the text,[29,36] eq A1 is rewritten as

$$mX_2 = m^{\mathrm{m,t}}X_2^{\mathrm{m,t}} + m^{\mathrm{V}}X_2^{\mathrm{V,t}} + m^{\mathrm{M}}X_2^{\mathrm{M,t}} \tag{A3}$$

where $m^{\mathrm{m,t}}$ is the monomer concentration and $X_2^{\mathrm{m,t}}$, $X_2^{\mathrm{V,t}}$, and $X_2^{\mathrm{M,t}}$ are the composition at the vesicle−micelle transition point. Putting $m^{\mathrm{M}} \rightarrow 0$ and considering the lever rule for the phase diagram of the monomer−vesicle equilibrium given by

$$m^{\mathrm{V}}/m^{\mathrm{m,t}} = (X_2 - X_2^{\mathrm{m,t}})/(X_2^{\mathrm{V,t}} - X_2), \qquad X_2^{\mathrm{m,t}} < X_2 < X_2^{\mathrm{V,t}} \tag{A4}$$

we have the concentration $m_{\mathrm{V}}^{\mathrm{V+M}}$ as

$$m_{\mathrm{V}}^{\mathrm{V+M}} = [X_2^{\mathrm{m,t}}/X_2 + (X_2 - X_2^{\mathrm{m,t}})X_2^{\mathrm{V,t}}/(X_2^{\mathrm{V,t}} - X_2)X_2]m^{\mathrm{m,t}} \tag{A5}$$

This is eq 12 in the text and the corrected version of eq 5 in our previous paper.[17] Similarly, putting $m^{\mathrm{V}} \rightarrow 0$ in eq A1 and using the lever rule for the phase diagram of the monomer−micelle equilibrium

$$m^{\mathrm{M}}/m^{\mathrm{m,t}} = (X_2 - X_2^{\mathrm{m,t}})/(X_2^{\mathrm{M,t}} - X_2), \qquad X_2^{\mathrm{m,t}} < X_2 < X_2^{\mathrm{M,t}} \tag{A6}$$

we have $m_{\mathrm{V+M}}^{\mathrm{M}}$ as

$$m_{\mathrm{V+M}}^{\mathrm{M}} = [X_2^{\mathrm{m,t}}/X_2 + (X_2 - X_2^{\mathrm{m,t}})X_2^{\mathrm{M,t}}/(X_2^{\mathrm{M,t}} - X_2)X_2]m^{\mathrm{m,t}} \tag{A7}$$

which is eq 13 in the text and the corrected one of eq 6 of our previous paper.[17]

References and Notes

(1) Laughlin, R. G. *The Aqueous Phase Behavior of Surfactants*; Academic Press: London, UK, 1997.

(2) Gelbart, W. M.; Ben-Shaul, A.; Roux, D. *Micelles, Membranes, Microemulsions, and Monolayers*; Springer-Verlag: New York, 1994.

(3) Evans, D. F.; Wennerström. *The Colloidal Domain*, 2nd ed; Wiley-VCH: New York, 1999.

(4) Talmon, Y.; Evans, D. F.; Ninham, B. W. *Science* **1983**, *221*, 1047.

(5) Matsumoto, T. *Colloid Polym. Sci.* **1992**, *270*, 492.

(6) Caria, A.; Regev, O.; Khan, A. *J. Colloid Interface Sci.* **1998**, *200*, 19.

(7) Kawamura, H.; Manabe, M.; Nomura, M.; Inoue, T.; Murata, Y.; Sasaki, Y. *Nippon Kagaku Kaishi* **1996**, *10*, 861.

(8) Svitova, T. F.; Smirnova, Y. P.; Pisarev, S. A.; Berezina, N. A. *Colloids Surf. A* **1995**, *98*, 107.

(9) Cantù, L.; Corti, M.; Favero, E. D.; Raudino, A. *J. Phys. II* **1994**, *4*,1585.

(10) Israelachivili, J. *Intermolecular & Surface Forces*, 2nd ed; Academic Press: San Diego, CA, 1991; p 378.

(11) Bergström, M. *J. Colloid Interface Sci.* **2001**, *240*, 294.

(12) Villeneuve, M.; Kaneshina, S.; Aratono, M. *J. Colloid Interface Sci.* **2001**, *239*, 254.

(13) Lusvardi, K. M.; Full, A. P.; Kaler, E. W. *Langmuir* **1995**, *11*, 487.

(14) Viseu, M. I.; Edwards, C. S.; Campos, C. S.; Costa, S. M. B. *Langmuir* **2000**, *16*, 2105.

(15) Viseu, M. I.; Velazquez, N. M.; Campos, C. S.; Garcia-Mateos, I.; Costa S. M. B. *Langmuir* **2000**, *16*, 4882.

(16) Treiner, C.; Makayssi, A. *Langmuir* **1992**, *8*, 794.

(17) Villeneuve, M.; Kaneshina, S.; Imae, T.; Aratono, M. *Langmuir* **1999**, *15*, 2029.

(18) Kaler, E. W.; Herrington, K. L.; Murthy, A. K.; Zasadzinski, J. A. N. *Science* **1989**, *245*, 1371.

(19) Kaler, E. W.; Herrington, K. L.; Miller, D. D.; Zasadzinski, J. A. N. In *Structure and Dynamics of Strongly Interacting Colloids and Supramolecular Aggregates in Solution*; Chen, S.-H., et al., Eds.; Kluwer Academic Publishers: Amsterdam, The Netherlands, 1992; p 571.

(20) Dragèviæ, D.; Bujan, M.; Grahek, Z.; Filipoviæ-Vincekoviæ, N. *Colloid Polym. Sci.* **1995**, *273*, 967.

(21) Tomašiæ, V.; Štefaniæ, I.; Filipoviæ-Vincekoviæ, N. *Colloid Polym. Sci.* **1999**, *277*, 153.

(22) Iampietro, D. J.; Kaler, E. W. *Langmuir* **1999**, *15*, 8590.

(23) Tondre, C.; Caillet, C. *Adv. Colloid Interface Sci.* **2001**, *93*, 115.

(24) Villeneuve, M.; Kaneshina, S.; Aratono, M. *J. Colloid Interface Sci.* **2003**, *262*, 227.

(25) Motomura, K.; Iwanaga, S.; Hayami, Y.; Uryu, U.: Matuura, R. *J. Colloid Interface Sci.* **1981**, *80*, 32.

(26) Lando, J.; Oakley, H. T. *J. Colloid Interface Sci.* **1967**, *25*, 526.

(27) Matsubayasi, N.; Motomura, K.; Kaneshina, K.; Nakamura, M.; Matuura, R. *Bull. Chem. Soc. Jpn.* **1977**, *50*, 523.

(28) Sakamoto, H.; Murao, A.; Hayami, Y. *J. Inst. Image Information Television Engneers* **2002**, *56*, 1643.

(29) Motomura, K.; Yamanaka, M.; Aratono, M. *Colloid Polym. Sci.* **1984**, *262*, 948.

(30) Matsubara, H.; Ohta, A.; Kameda, M.; Ikeda, N.; Aratono, M. *Langmuir* **2000**, *16*, 7589.

(31) Sadar, M. *Technical Information Series*, Booklet No. 11; Hach Company: USA, 1998.

(32) Hunter, R. J. *Introduction to Modern Colloid Science*; Oxford University Press: England, UK, 1993.

(33) Belkoura, L.; Stubenrauch, C.; Strey, R. *Langmuir* **2004**, *20*, 4391.

(34) Stroscio, J. A.; Kaiser, W. J. *Scanning Tunneling Microscopy*; Academic Press: San Diego, CA, 1993.

(35) Murakami, R.; Takata, Y.; Ohta, A.; Takiue, T.; Aratono, M. *J. Colloid Interface Sci.* **2004**, *270*, 262.

(36) Aratono, M.; Villeneuve, M.; Takiue, T.; Ikeda, N.; Iyota, H. *J. Colloid Interface Sci.* **1998**, *200*, 161.

(37) Manabe, M. In *Surfactant Science Series*; Esumi, K., Ueno, M., Eds.; Marcel Dekker: New York, 2003; Vol. 124, p 93

(38) Dubois, M.; Zemb. T. *Langmuir* **1991**, *2*, 1352

(39) Marques, E. F.; Regev, O.; Khan, A.; Miguel, M. G.; Lindman, B. *J. Phys. Chem. B* **1999**, *103*, 8353.